Proceedings World Geothermal Congress 2020+1
Reykjavik, Iceland, April - October 2021

A Review of Casing Failures in Geothermal Wells

P. V. Suryanarayana, Ravi M. Krishnamurthy, Udaya B. Sathuvalli and John Bowling

Blade Energy Partners, 2600 Network Blvd., Suite 500, Frisco, Texas 75034, USA

pvsury@blade-energy.com

Keywords: Casing design, Casing failure, Collapse, Inelastic buckling, Annular Pressure Buildup, Geothermal Well Integrity

ABSTRACT

Lifetime well integrity of geothermal wells is an important consideration in the development of geothermal resources. Despite its importance, coverage of this topic in the literature and standards is limited. Indeed, Working Stress Design (WSD) remains the basis of tubular design in geothermal wells, driving designers to select higher yield strength materials to satisfy the large cyclic thermal loads. Materials selection is usually driven by corrosion considerations, sometimes leading to the selection of expensive corrosion resistant alloys. Unfortunately, wells continue to fail even with high strength or CRA materials. Use of lower yield strength materials is desirable because of the higher ductility and increased fatigue life. However, this implies acceptance of yielding. In a previous work (Suryanarayana and Krishnamurthy, 2018), the authors have demonstrated the use of a post-yield, low cycle fatigue based design approach to improve lifetime well integrity of geothermal wells. Post-yield design addresses some of the major threats to well integrity in geothermal wells: low cycle fatigue, brittle failure, and connection failures. However, there are other concerns in well integrity, often manifesting in the early life of a well, that should be addressed in a complete design. These include tension-collapse (or "cold collapse"), inelastic buckling of short unsupported sections, and collapse induced by trapped annular pressure, resulting in integrity issues such as tubular failures and leaks.

Tension-collapse or cold collapse conditions occur due to the combination of high tension and a collapse load. This mode of loading occurs in the cold half cycle. A design check to cover this load scenario is described in the paper. Short unsupported sections are sites for inelastic buckling. It is shown in this work that inelastic buckling during the heat half cycle, followed by tensile parting during cool down, can potentially cause kinks or tensile failures in such locations, even though the tubular may satisfy working stress or post-yield design criteria. A mathematical approach to calculating the maximum allowable temperature to avoid such failures is presented. Collapse may also occur due to trapped fluid pressure during the hot half cycle. This failure mode is more difficult to mitigate by design. Therefore, carefully planned cementing strategies to avoid the creation of trapped fluid pockets may be the only rational approach. Well architecture modifications that can mitigate this failure mode are also discussed.

Finally, despite appropriate design, tubulars may succumb to various corrosion mechanisms. The paper discusses typical corrosion mechanisms in geothermal wells, and presents an approach to analyze corrosion and consider it in the design of tubulars, and in the selection of materials. The use of thermodynamic and thermohydraulic simulation tools to establish the phase behavior and estimate the rate of corrosion (and hence loss of wall) is discussed. The methods described are illustrated with practical examples. The information provided in this paper offers an additional basis for design of geothermal wells to improve lifetime well integrity.

1. INTRODUCTION

Geothermal (and steam injection thermal service) wells are subjected to cyclic thermal loading at very high temperatures. In geothermal wells, producing temperatures can reach 600°F (316°C), and in superhot and supercritical geothermal wells, are well in excess of this. Cool down to undisturbed geothermal temperature can occur when wells are shut-in. The cool down is further increased during the quenching operation. As the casings are axially constrained, the high producing temperatures lead to very high compressive thermal stresses during the heat half cycle. If traditional Working Stress Design is used, it would drive the selection of high strength tubulars. Tubular materials with high yield strength have substantially lower ductility when compared with low grade materials, and correspondingly lower fatigue life. They also possess low brittle failure resistance, contraindicating their use in sour service conditions. On the other hand, using lower yield materials implies acceptance of compressive yielding, and corresponding high tensile stresses upon cool down.

The benefit of using lower yield strength materials in thermal service wells is well understood, and well-articulated in the literature (Holliday, 1969; Lepper, 1998; Suryanarayana and Krishnamurthy, 2015, Han, et. al., 2018). In general, these "post-yield" methods allow compressive yielding of both pipe body and connections, but limit the extent of yielding such that the additional tensile stress upon cool down, and the fatigue damage from cycling between the high and low temperatures, are within acceptable limits. Although the commonly used standard, the New Zealand Standard NZS 2403:2015, does not cover it in detail, it mentions the use of post-yield design as acceptable in geothermal wells. The recommended practice document IRP, Volume 3 (2002), commonly used for the design of steam thermal service wells, has long allowed the use of post-yield design for thermal service tubulars. Post-yield design approaches such as strain-based design and low cycle fatigue design are now common in geothermal and thermal service well design (Holliday, 1969; IRP Vol 3, 2002, Suryanarayana and Krishnamurthy, 2018, Han, et. al., 2018).

Holliday (1969) first described a post-yield design basis for thermal service tubulars. Suryanarayana and Krishnamurthy (2015, 2018) describe two post-yield approaches to design thermal service tubulars and connections. In the modified Holliday approach (MHA), which is based on the original post-yield approach described by Holliday, compressive yield is allowed during the heat half-cycle. However, the extent of post-yield strain is limited such that the tensile stress upon cool down is no greater than the yield strength of the material. However, Holliday considered only ideal elastic-plastic material behavior in his work. In the modified approach, cyclic strain hardening, Bauschinger effect, and Thermal relaxation (creep like behavior) are taken into account. The design criterion is to ensure that the ratio of the triaxial (von Mises Equivalent) stress to the yield strength, known as the Holliday

Stress Ratio (HSR), is lower than an allowable maximum. The allowable maximum is a function of the material grade. For K55 the recommended allowable maximum is 1.6, and for L80, it is 1.4. The lower ratio for L80 is an allowance for lower ductility in the higher yield material.

In the Low Cycle Fatigue (LCF) approach, fatigue damage from plastic strain cycling is accumulated using a Ductile Failure Damage Indicator or DFDI (Hancock and McKenzie, 1976; Fischer, et. al., 1995), with a "critical strain" as the reference strain (Gao and Krishnamurthy, 2015). The critical strain is lower than the failure strain and represents the strain at which micro voids in the material microstructure coalesce, leading to the formation of an incipient crack. All plastic strain events are counted in the damage accumulation. The design criterion ensures that the accumulated fatigue damage is less than unity. The LCF approach also allows consideration of connections, sour service (H_2S exposure), and geomechanically induced displacements, as discussed briefly below. Krishna, et. al. (2018) reported on the experimental validation of the use of DFDI approach in LCF design. Case studies using the modified Holliday Approach and the LCF approach for both thermal service and geothermal wells are presented by Powers, et. al., (2016). The case studies cover both pipe body and connection designs. Using the LCF approach, Powers et. al. show that connection fatigue life is lower than pipe body fatigue life, sometimes substantially so, depending upon the type of connection used.

Connections act as strain localization elements in the casing. In general, as noted by Powers, et. al. (2016), connections in thermal service tubulars experience local strains greater than the strains in the pipe body, and therefore can be the weak link(s) in well integrity. This is important to recognize, since the peak stress (and strain) in the connections may be beyond yield even if the pipe body stress and strain are below yield limits. As a result, even though pipe body fatigue life may be high, fatigue life of commonly used OCTG connections may be low due to cyclic plastic strain, leading to premature connection failures. Teodoriu and Falcone (2008) provide experimental results showing that the connection fatigue life is much lower than the pipe body fatigue life. A novel connection design to limit strain localization, by allowing thermal expansion within the connections while maintaining a gas seal, was introduced by Thorbjornsson, et. al. (2017).

Connection qualification for thermal service follows the ISO/PAS 12835:2013 protocol. This protocol has been specifically developed for thermal service connections that see cyclic temperatures well in excess of 180°C. Four application service levels are defined in the protocol, all the way to ASL 350, at which connections are tested for a minimum of ten cycles at 350°C. However, qualification testing in conformance to the ISO/PAS 12835:2013 protocol is expensive and time consuming, which is why very few connections have been qualified by using this protocol. An alternative approach is described by Suryanarayana and Krishnamurthy (2018). In this approach, a Finite Element Analysis of the connection and pipe body are conducted to arrive at a Strain Localization Factor, which is then used in the Low Cycle Fatigue format. The resulting connection fatigue life is usually much lower than pipe body fatigue life. Nevertheless, if this method is used, as long as the connection fatigue life is in excess of the functional requirements of the well, the design is adequate. Powers, et. al. (2016) provide examples of applying this approach to connection design in actual case studies. In general, results indicate that proprietary connections provide more life than API Buttress connections. This is also the finding of Teodoriu and Falcone (2008) and Maruyama, et. al. (1990).

In sour service wells, where exposure to H_2S is expected at low temperatures, brittle failure from sulfide stress cracking can dominate. In general, low grade materials, such as K55 and L80 that are commonly used in geothermal wells, have high resistance to sulfide stress cracking. Coupled with the high temperatures, brittle failure from sulfide stress cracking is rare in geothermal wells. Nevertheless, fatigue life of strain-hardening materials can be affected when exposed to H_2S. In the context of the LCF design approach, the critical strain reduces in sour service environments, thus reducing available life. The extent to which the critical strain reduces depends upon the grade and the partial pressure (solubility) of properly partitioned H_2S.

In geothermal and thermal service wells, geomechanically induced displacements are sometimes a cause for concern. Subsidence (and compaction), and lateral displacements induced by movement of formations can impose additional strain on the casing. In the LCF approach, this strain is calculated and included in the total strain when calculating the accumulated damage.

Post-yield design approaches enable the use of lower grade tubulars in high temperature applications, and provide a basis for safe design of tubulars. The most common grades used in geothermal and thermal service design are K55 and L80, and occasionally, T95. Corrosion concerns may drive selection of other materials, but it should be borne in mind that ductility is very important for the integrity of thermally cycled tubulars. When casing is properly designed using one of the above discussed post-yield design methods, it is reasonable to expect that the basic mechanical design is adequate, and fatigue failure, tensile failure, or connection failure are consequently managed appropriately to ensure well integrity. Nevertheless, these methods do not cover all of the failure mechanisms that could cause failures, which need to be considered separately.

Literature on geothermal well integrity and failures is limited. Teodoriu (2015) presents a discussion of why casings fail in geothermal wells, and in particular focuses on connections and local buckling. An excellent review of geothermal well failures is provided in Kruszewski and Wittig (2018). Although this work primarily reviews superhot and supercritical geothermal well failures, the coverage is wide enough to provide a valuable basis for considering different failure mechanisms. Southon (2005) also provides an excellent discussion of casing failure modes in geothermal wells, and their design implications, focusing in particular on casing "implosion" and compressive failures. Lentsch, et al (2015) provide a discussion of geothermal well casing failures in Germany, and highlight three main causes, including APB induced collapse.

In this work, we focus on one of the more common classes of failure reported in geothermal wells – collapse. By collapse, we mean any failure that causes inward deformation of the casing, compromising drift and operability of the well, and in some cases, leading to failure of the casing. Different mechanisms of collapse-like failure are discussed– cold collapse, inelastic buckling, and APB induced collapse. All of these have been reported in the literature, and need to be considered separately. Additionally, since wall loss (whether from corrosion or casing wear) affects all these collapse failure mechanisms, an approach to incorporate wall loss in the design is also discussed.

2. COLD COLLAPSE

2.1 Description

"Cold Collapse" refers to the combination of high tension with a collapse load, which can occur in geothermal and thermal service wells in the cold half cycle. The post-yield basis of design for thermal service tubulars allows compressive yielding of the pipe during heat-up (production). A consequence of this compressive yielding is a high residual tension in the pipe upon cool down (to ambient upon shut-in, or during quenching). Depending upon the magnitude of the temperature change and the grade of the casing, this tensile stress can be at or beyond the yield strength of the material. Moreover, the tensile stress can increase in each successive cycle due to cyclic strain hardening, which is exhibited by typically selected casing grades. Figure 1 illustrates the cyclic behavior of typical casing grades when subjected to constant strain (fully reversed) thermal cycles. The temperature increase is such that compressive yielding occurs during heat-up. The consequent tensile stress is close to yield in the first cycle, and due to cyclic strain hardening, exceeds yield in the second cycle. Thus, upon cool-down, high tensile stress is a given if compressive yielding is allowed during heat-up. Most geothermal well applications belong to this category.

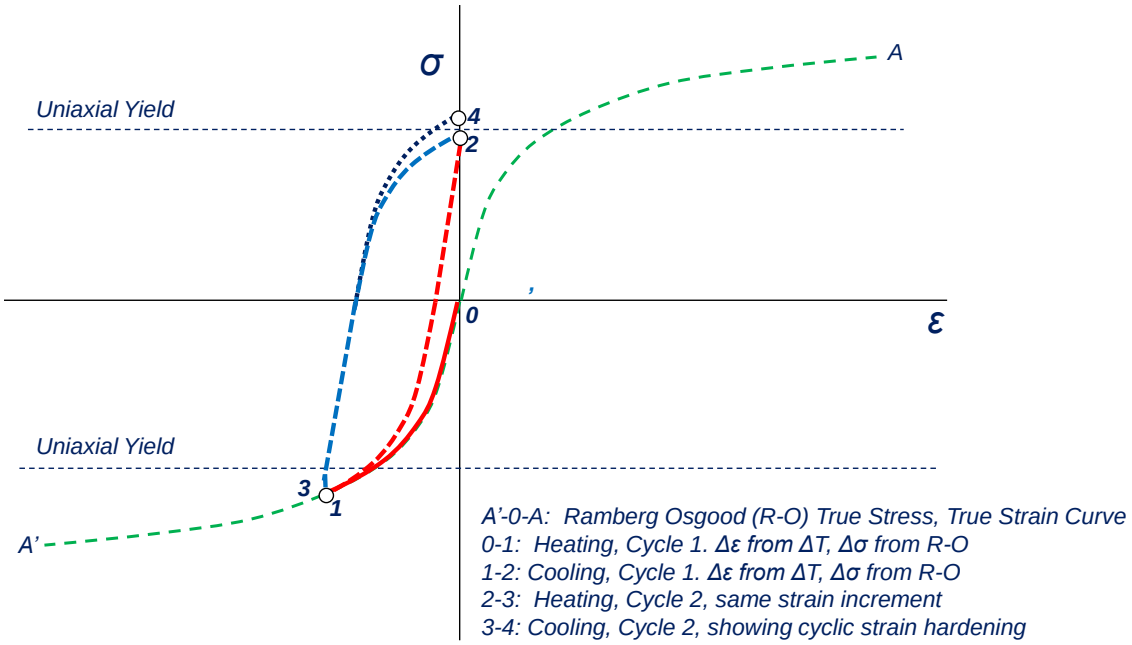

Figure 1: Cyclic behavior under constant strain thermal cycling, showing hysteresis and cyclic strain hardening.

If the casing is then subjected to a collapse load upon cool down, a combination of high tension and collapse can occur. In geothermal wells, a collapse load can arise after shut-in, since the water level in the well can be quite deep, leaving a considerable length of the production casing or tieback fully evacuated. Since tension reduces the collapse strength, this combination of loading can lead to conditions favorable to a collapse failure if the casing is not appropriately designed.

2.2 Maruyama, et. al. Experimental Work

The "Cold Collapse" mechanism was first investigated by Maruyama, et al. (1990), who performed collapse tests on casing under extremely high tension loads. They conducted collapse tests on 5.510 in. (140 mm) OD K55 casing, with two different wall thicknesses (0.197 in. or 5 mm, and 0.299 in. or 7.6 mm), to simulate a "thin wall" and a "thick wall" case. These samples were machined to uniform pipe, to exclude effects of ovality and eccentricity. In addition, they also tested a 7 in. (178 mm) OD, 0.378 in. (9.6 mm) N80 pipe sample. In the tests, an axial load was applied to the test sample in a biaxial collapse test apparatus, and the external pressure was increased until the casing collapsed. By varying the axial load and repeating the experiment, a biaxial collapse resistance curve for the tested samples was obtained. Maruyama, et. al., unfortunately do not describe the end condition of the apparatus. This can be important. If the ends are fixed (zero displacement boundary condition) after applying the axial load, the applied external pressure serves to reduce the axial stress due to the Poisson effect. If on the other hand, the axial load is maintained constant at the initial applied magnitude throughout the test (constant axial load boundary condition), the axial stress remains constant. These two boundary conditions result in very different collapse resistance behavior, as will be discussed shortly. Nevertheless, Maruyama, et. al.'s results are very important for understanding cold collapse. To the authors' best knowledge, these tests are possibly the only published experimental study of high tension-collapse behavior of steel pipes, with tension in excess of yield.

The experimental results of Maruyama, et. al., are reproduced below as Figure 2. This figure compares the collapse performance of the two 5.510 in. OD, K55 samples, with wall thickness of 0.197 in. and 0.299 in., respectively "thin wall" and "thick wall" cases. For reference, the API Collapse for the thin wall pipe is 13.38 MPa (Transition Collapse Regime), and the API Collapse for the thick wall pipe is 32.83 MPa (Plastic Collapse Regime) In Figure 2, the *y* axis is the collapse strength, while the *x* axis is the applied axial tensile stress. The solid curves in the figure represent the calculated VME-based collapse strength. The API biaxial correction for tension uses a VME-based adjustment to the yield strength based on applied tensile stress, as follows:

$$\sigma_{YPa} = \left(\sqrt{1 - 0.75(\sigma_{axial} / \sigma_{YP})^2} - 0.5\sigma_{axial} / \sigma_{YP} \right) \sigma_{YP} \quad (1)$$

In the above equation, σ_{YPa} is the yield strength adjusted for axial tension, σ_{axial} is the axial tensile stress, and σ_{YP} is the original (unadjusted) specified minimum yield strength of the pipe. It is customary to apply this only when tensile stress is present. The adjusted yield strength σ_{YPa} is then used in place of the original yield strength in calculating the collapse strength. A cursory review of the above Eq. (1) shows that when the axial stress is equal to the yield strength, the adjusted yield strength is zero. This essentially implies that there is no more collapse resistance when the tensile stress is at (or by inference, beyond) the yield strength of the material. For this reason, the solid curves in Figure 2 reach zero at yield strength. However, as Figure 2 shows, collapse strength does not go to zero even when the axial stress is beyond yield. Indeed, API TR 5C3 (2008) specifically indicates that the API Collapse equations should not be applied for high tensile stresses. Therefore, a more appropriate design basis is required for examining casing integrity under "Cold Collapse" load condition.

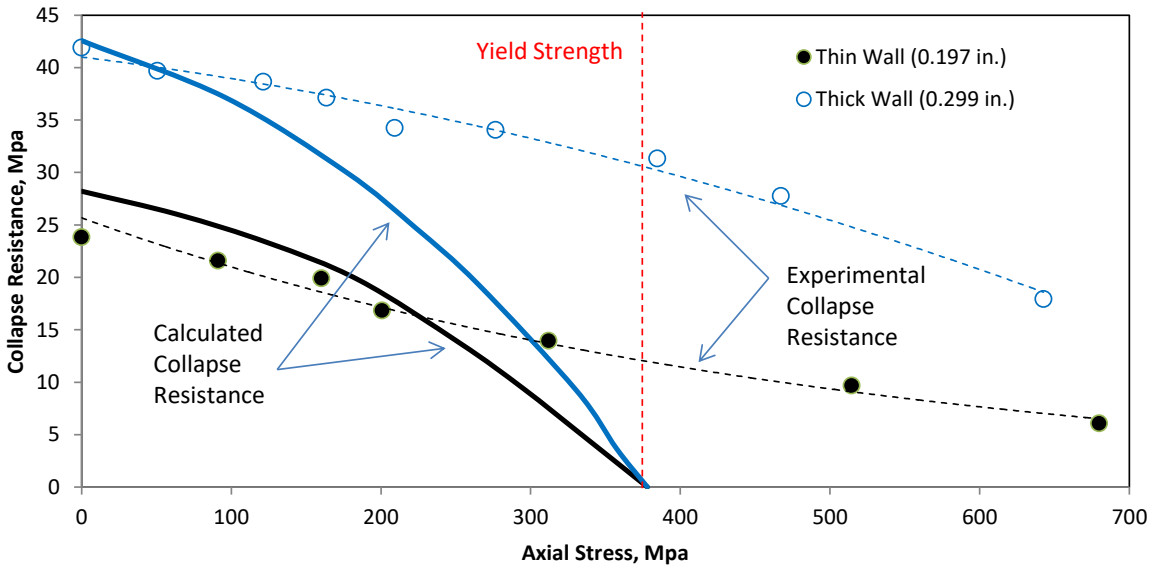

Figure 2. Experimental determination of collapse strength under high axial stress for 5.51 in. OD, K55 pipe samples (After Maruyama, et. al., 1990)

2.3 Toscano and Dvorkin FEA Results

Toscano and Dvorkin (2011) conducted finite element simulations of collapse under high tensile stress for pipes similar to those tested by Maruyama, et. al. They considered 7 in. OD, K55 and L80 grade pipes (the assumed wall thickness is not mentioned, but can be inferred from their results as 0.317 in., or 23 lb/ft weight). The *D/t* of this pipe is 22.1, and the API Collapse strength is 22.55 MPa (Plastic Collapse Regime). Figure 3 shows their results for the K55 grade pipe. In this figure, crucially, they consider both the zero displacement end condition (Displacements applied) and the constant axial stress end condition (Loads applied).

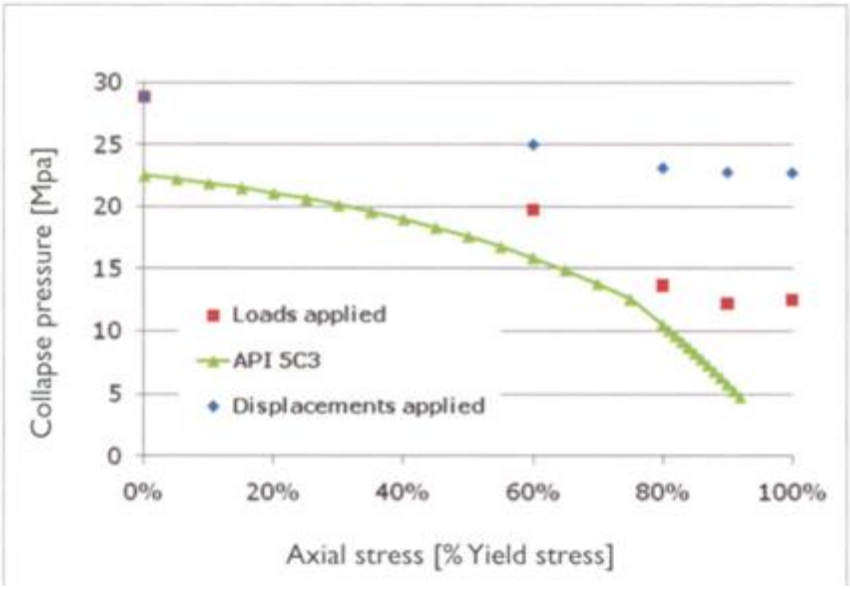

Figure 3. Collapse Strength FEA Results from Toscano and Dvorkin (2011)

Several key conclusions can be drawn from this work:

- Collapse resistance at high tensile stresses is significantly higher than the pressure predicted by the API Collapse equation.
- Collapse resistance with the zero displacement end condition is greater than with constant axial stress end condition. The zero displacement end condition is probably more representative of casing axially constrained by cement. Nevertheless, for design, it is more conservative to consider the constant axial stress condition.
- The constant axial stress end condition results are in line with Maruyama et. al.'s experimental results, although the size and wall thickness investigated by Toscano and Dvorkin are not the same as the sizes for which Maruyama et. al. report collapse performance with axial stress.

2.4 Benchmarking FEA Results

In order to obtain a basis for inference and for presenting a basis of design for cold collapse, the authors performed benchmarking finite element analyses to compare with both Maruyama et. al. and Toscano and Dvorkin. The FEA model was constructed in ABAQUS. The true stress-true strain material curve is used directly in the analysis (see Figure 4), rather than make assumptions about hardening. This curve is based on experimental data gathered on several K55 samples.

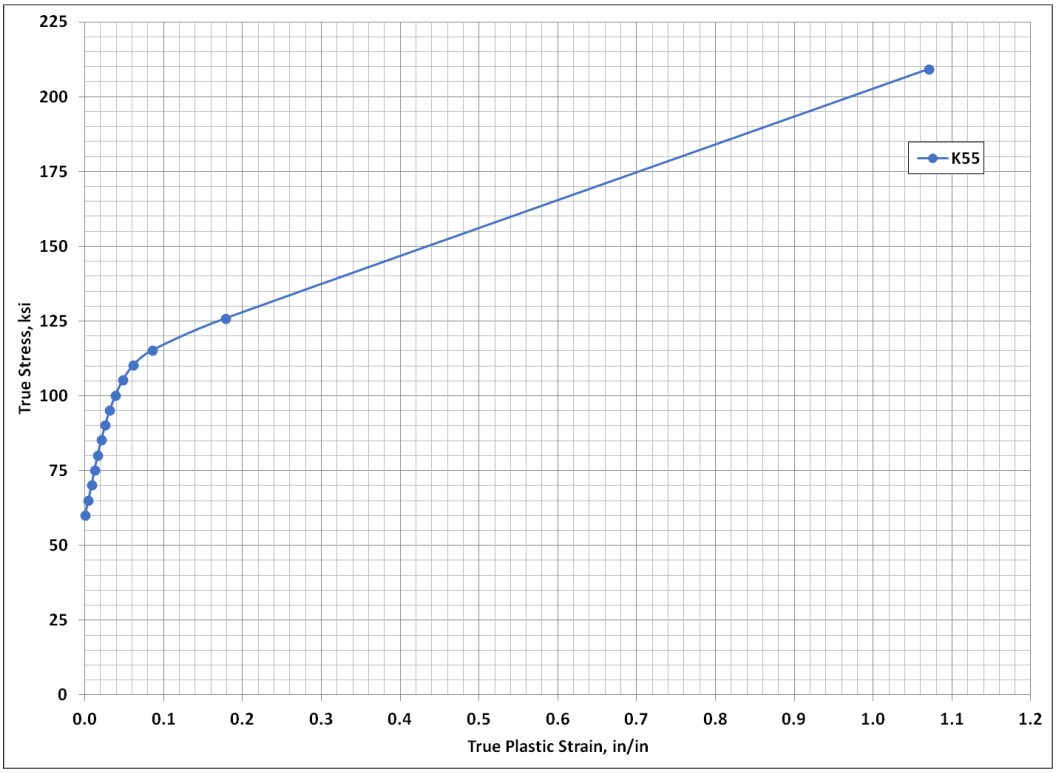

Figure 4. True Stress – True Strain Curve for K55

The FEA model had the same length to OD ratio (10) as the model used by Toscano and Dvorkin. Eight noded brick elements of 0.25 in. size are used, with four elements across the wall thickness. Two end conditions are simulated: axially constrained pipe; and a pipe with applied constant axial strain. External pressure is then steadily increased in steps until numerical instability occurs in the model, which is interpreted as collapse. The results are summarized in Table 1.

Table 1. Comparison of FEA results with previous work

7 in. OD, 23 lb/ft (0.317 in. wall), K55			5.51 in. OD, 0.197 in. wall, K55			
	Collapse Strength, MPa			Collapse Strength, MPa		
Axial Stress, Mpa	This Work	Toscano & Dvorkin	Axial Stress, Mpa	This Work, Const Load	This Work, Zero displ	Maruyama, et. al.
0.00	37.78	28.80	0.00	30.09	30.23	28.28
113.08	37.01	23.83	100.00	29.83	28.30	21.20
226.16	28.03	19.80	200.00	20.94	23.15	17.15
374.68	14.02	12.70	330.00	9.06	20.23	13.53
481.86	12.56	N/A	515.00	6.92	20.05	9.73

In the first panel of Table 1, the results of our FEA are compared to those of Toscano and Dvorkin, for a 7 in. OD, 0.317 in. wall, K55 pipe. Both these results are with constant applied axial load. In general, Toscano and Dvorkin's results are lower than our FEA results, although the results are closer at higher tensile stress. One reason for this difference is our use of the true stress – true strain curve, whereas Toscano and Dvorkin used a 55 ksi yield with a tangent modulus to model to represent hardening. In terms of

percent of original collapse strength remaining, our model calculates 33% of original collapse remaining at 481.86 MPa axial stress. At a tensile axial stress of 374.68 Mpa, the last point where results are available for both analyses, the ratio is 37.1% for our work, and 44.1% for Toscano and Dvorkin's work.

In the second panel of Table 1, the results of our FEA with both constant applied load and zero displacement end conditions for a 5.510 in. OD, 0.197 in. wall, K55 pipe are compared to the experimental results of Maruyama, et. al. for the same pipe. Although Maruyama et. al. do not describe their end conditions in detail, it would appear that they correspond to the constant axial load end condition. The collapse strength calculated using FEA for the zero displacement end condition are substantially higher, with moderate loss of collapse strength with increasing axial stress, behaving in the same way as Toscano and Dvorkin's results for the zero displacement end condition. The results of Maruyama et. al. agree reasonably well with the FEA results. In terms of percent remaining collapse strength, our results (for constant applied axial load) show 23% remaining strength at 515 MPa, while Maruyama et. al.'s experiments show 34% remaining strength at the same axial stress. The FEA model could not be run at higher axial loads due to numerical instability with near zero external pressure (implying zero collapse strength). Nevertheless, this suggests that for the thin wall case, our results for the constant axial stress end condition are in general agreement with Maruyama's results, and are more conservative at higher values of axial stress.

2.5 Design Basis for Cold Collapse

If the application temperature and material choice is such that the material does not yield in compression (implying application temperature less than 160°C for K55, and less than 216°C for L80), the material does not yield in the heat half cycle, and therefore does not develop residual tension upon cool down. In this case, the full API collapse resistance is available, and the standard API approach can be used for collapse design. In most such cases, the collapse resistance of the typical casing and tieback strings far exceeds the collapse load, and collapse is unlikely to dictate design.

However, when the application temperature exceeds the above mentioned yielding conditions, the casing material yields in compression during the heat half cycle, and develops high residual tension during cool down. Such a development of high residual tension is common in geothermal and thermal service wells. In this case, as discussed earlier, the API Collapse equations are not applicable, as the calculated collapse grossly underestimates the available collapse resistance. This inadequacy calls for a new basis of design to avoid the cold collapse failure mode. In what follows, a simple basis for design is discussed.

Table 2 shows the experimental results of Maruyama, et. al., (1990), extracted from their plot. Two sets of data are shown, both for 5.510 in. OD, K55 pipe. The High *D*/*t* data set is for a wall thickness of 0.197 in. (*D*/*t* = 28), referred to as ""Thin Wall" case by Maruyama et. al. The Low *D*/*t* ("Thick Wall") set is for a wall thickness of 0.299 in. (*D*/*t* = 18.4). It should be noted that *D*/*t* ratios greater than 20 are generally accepted as thin wall, while *D*/t ratios less than 15 are treated as thick wall pipes. In Table 2, the Axial Stress and Collapse Strength columns show the experimental results. The Collapse Ratio is the ratio of the experimentally determined collapse strength at a non-zero axial stress to the experimentally determined collapse strength with zero axial stress. For reference, the API Collapse for the High *D*/t pipe is 13.38 MPa (Transition Collapse Regime), and the API Collapse for the low *D*/*t* pipe is 32.83 MPa (Plastic Collapse Regime). For both cases, the experimentally determined collapse strength is higher than the API collapse at zero axial stress. This is likely because the pipes used in the experiment were machined to uniform wall thickness, so that eccentricity and ovality are negligible. For this reason, we believe it is more reasonable to take the ratio with respect to the experimentally determined collapse strength at zero axial stress, rather than using the API collapse with zero axial stress.

Table 2. Experimental Data of Maruyama, et. al. (1990)

High D/t (Thin Wall) Pipe			Low D/t (Thick Wall) Pipe		
Axial Stress (Mpa)	Collapse Strength (Mpa)	Collapse Ratio	Axial Stress (Mpa)	Collapse Strength (Mpa)	Collapse Ratio
0.0	28.28	1.00	0.0	41.92	1.00
4.6	23.74	0.84	5.5	41.58	0.99
98.5	21.21	0.75	49.1	39.90	0.95
164.0	19.87	0.70	128.0	38.38	0.92
204.2	16.84	0.60	171.6	37.04	0.88
316.7	13.80	0.49	208.5	34.34	0.82
521.5	9.60	0.34	284.1	34.18	0.82
675.9	5.89	0.21	391.5	31.14	0.74
			475.4	27.78	0.66
			641.3	18.18	0.43
			694.8	14.31	0.34

Based on these results, the following observations can be made:

- Even at the maximum applied axial stress (about 1.8 times the specified minimum yield stress), collapse strength does not go to zero, regardless of the *D*/*t* ratio.
- It is apparent that the thicker wall pipe retains more of its original (zero axial stress) collapse strength than the thin walled pipe at the maximum stress. This is not unexpected, since the mechanism of collapse is different in the two cases. In thick walled pipe, yield is governed by the VME criterion, whereas for the thinner wall, collapse is governed by elastic instability.

- Further, regardless of wall thickness or magnitude of axial stress, *at least 20% of the original collapse strength* is remaining. This is true even considering the FEA results, which in general show much higher remaining collapse strength when displacement is constrained, as is likely the case in a real well with a cemented tubular.

From the preceding discussion and observations, a conservative, and easily implemented, design basis is to assume that upon cool down, at least 20% of the original collapse strength is available in design for the cold collapse load. The design criterion is then to seek a collapse safety factor of at least 5 in standard design for cold collapse load. The load is set up as mud hydrostatic outside and zero internal pressure up to water level, and water gradient thereafter. This is arguably conservative, but appropriate for quick design checks. A more accurate, and complex, approach would be to conduct FEA for each well design. Alternatively, an analytical approach based on externally applied loads on concentric cylinders can be developed for both thick wall and thin wall cases, and can be used for a less conservative design basis. Sathuvalli, et. al. (2019) describe such an approach for arbitrary external loading of concentric cylinders. Although that work focuses on asymmetric external loading more appropriate for geomechanically induced displacements or salt loads, it can be modified to suit the current problem. This work is ongoing at the time of this writing.

2.6 Example

An example will best serve to illustrate the approach. Consider a geothermal well with a 9 5/8 in., 47 lb/ft (0.472 in. wall) L80 production tieback. This string has an API Collapse strength of 4,750 psi (32.76 MPa). The tieback runs from surface to 850 m (top of first production liner). The maximum temperature at the wellhead during production is 300°C, implying that the casing will definitely yield in the heat half-cycle, and will pick up a corresponding residual tension upon cool down. The cold collapse design check is therefore appropriate for this well.

Assume that the section was drilled with 1.08 SG mud. Further, assume that the water level during cool down is at 870 m. This leaves the entire tieback evacuated. Performing the design check at 850 m, the mud hydrostatic is 1,305 psi (9 MPa). This is the external pressure, and the internal pressure is zero (assuming negligible gradient in the non-condensable gases above water level). This gives a "Cold Collapse" load of 1,305 psi (9 MPa). The safety factor (API collapse strength divided by the cold collapse load) is then 3.64, below the 5 required as per the design basis described in the preceding section. This means that the string is susceptible to cold collapse failure. If the weight is increased to 53.50 lb/ft (0.545 in. wall), the API collapse strength increases to 6,620 psi (45.66 MPa), and the safety factor for the cold collapse load is now 5.07, just satisfying the design criterion. The alternative of increasing the grade does not provide adequate collapse resistance, not to mention the risk associated with selecting a grade higher than T95 in a cyclic thermal service well.

2.7 Discussion

It is important to check the cold collapse load case in all geothermal well designs. It may well drive the design. If the cold collapse design check as described above does not pass, the simple expedient of increasing the wall thickness (or grade, if possible) usually solves the problem. Kruszewski and Wittig (2018) describe a casing collapse experienced in the Nisyros-1 geothermal well in Greece. In this well, collapse was experienced over a significant length of the 9 5/8 in. production casing. After repair and installation of 7 in. tieback casing, the problem reoccurred in the 7 in. casing as well. Kruzewski and Witting suggest that the rapid heating during production (400°C flowing wellhead temperature) followed by cooldown during cold water quenching was the cause of the failures. It was reported that a neighboring well using a higher yield strength material for a similar application did not suffer the same problem. This is suggestive of cold collapse. Similar cold collapse cases have been investigated by the authors on behalf of geothermal operators in the past.

The typical characteristics of cold collapse failure may be summarized as follows:

- The collapse occurs in the cold condition, and may occur after multiple cycles have passed. This is because the residual tensile stress can increase in each cycle due to cyclic strain hardening (Lepper, 1998; IRP-3, 2002).
- The collapse occurs along a long section of pipe, and looks similar to classical hydrostatic collapse.
- The collapse occurs when water level is deep, creating a larger collapse load on the incident tieback or liner.

3. INELASTIC BUCKLING

The traditional basis for thermal and geothermal well construction is to cement all casing strings to surface (and liners to the hanger). However, un-cemented intervals can occur in open hole sections, non-vertical sections, and even in tiebacks. These un-cemented sections must be taken into account in casing design. An un-cemented section is unsupported, and hence can be a location for strain localization. Thermally induced compression can result in buckling, which, depending upon the length of the unsupported section, can be elastic or inelastic. Due to the high bending stresses that result from inelastic buckling, short cement gaps are dangerous to well integrity. Although strictly a "compressive" failure mode, inelastic buckling is included in this work due to its collapse-like appearance, and its frequent combination with APB induced collapse.

3.1 Transition from Elastic to Inelastic Buckling

In general, un-cemented sections are handled by including the post-buckling bending stress in the triaxial (VME) stress calculation, assuming that buckling is elastic. Most design programs include this calculation for elastic buckling. However, elastic buckling is possible only if the length of the unsupported section is slender (*i.e.*, long enough to allow elastic buckling). An unsupported section of length L_u is slender if

$$\frac{L_u}{2R_g} \geq \pi\sqrt{\frac{E}{\sigma_y}}\ ,\ R_g = \sqrt{\frac{I}{A_s}} \tag{2}$$

where R_g is the radius of gyration, I is the moment of inertia and A_s is the cross sectional area, in consistent units. In practice, at least two times the length calculated using Eq. (2) is considered the point from which pure elastic buckling occurs.

When the unsupported section is such that it can be treated as a slender tubular, buckling is initiated when the axial force exceeds the critical elastic buckling limit of the pipe. Given the high temperatures expected in thermal service wells, the thermal compression is always in excess of the critical buckling force, and the pipe is helically buckled. Helical buckling and post-buckling of radially constrained pipe is well understood, and has been addressed by several previous works (see, for example, Lubinski et. al., 1962; Mitchell, 1988). The main consequence of helical buckling is that the VME stress now includes the post-helical bending stress, and thus the total stress is greater than for an unbuckled (or fully supported) pipe for the same temperature increase. Therefore, the Holliday Stress Ratio is greater, as is the total strain in the LCF approach.

3.2 Inelastic Buckling Limit

Typical cement shortfalls are long enough that the unsupported section is slender. However, when the cement gaps are short or there are cement holidays due to poor cementing practices or top jobs, inequality (2) is not satisfied, and the unsupported section is no longer slender. In such cases, inelastic buckling can occur, due to eccentricity in the application of the axial force, causing a moment. The axial compressive stress at which inelastic buckling occurs may be estimated using the Secant formula,

$$\sigma_{\max} = \frac{F_c}{A_s}\left[1+\frac{e}{s}\sec\left(\frac{L_u}{2R_g}\sqrt{\frac{F_c}{A_s E}}\right)\right] \tag{3}$$

where $s = 2R_g^2 / OD$, and e is the eccentricity (in axial load application), which is an assumed quantity. A typical value for e is 0.3 in.

The direction of inelastic buckling (inward, resembling local collapse, or outward, resembling a bulge) depends upon the direction of differential pressure at the time of buckling. Inelastic buckling can also be “one sided”, that is, limited to a small azimuthal section of the pipe, if the unsupported section is on one side of the pipe, or if one side of the pipe has preferentially corroded and lost wall. For extremely short unsupported sections, this can appear like a lateral kink in the pipe. Figure 5 illustrates the different forms of inelastic buckling.

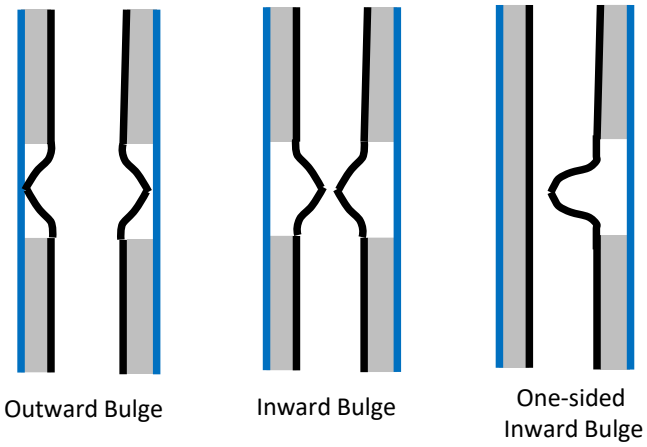

Figure 5. Illustration of Inelastic Buckling

An example of experimentally induced inelastic buckling is given by Teodoriu (2015). The figure from his work is reproduced here for reference as Figure 6. In some well designs, the use of API connections with a gap between the nose of each joint of casing can mask the overload from compression, which manifests as some connection gaps closing while other connection gaps widening and resulting in leaking joints. A common solution to this is changing the connection to a proprietary or “semi-premium” connection, where the gap is eliminated in the connection. When wells are put on production and the gap in the connection no longer accommodates the thermal expansion in an un-cemented interval, inelastic buckling results in damage similar to that shown in Figure 6.

Figure 6. Example of local inelastic buckling (after Teodoriu, 2015)

3.3 Design Approach

The effect of inelastic buckling can be included in the Modified Holliday Approach as follows:

- Determine if the unsupported length is slender (in design, at least 2 times the helical pitch of elastic buckling)
- If unsupported length is non-slender,
    - Assume an axial force, and use Eq. (3) to calculate the maximum allowable axial stress to initiate inelastic buckling (all other parameters being known).
    - Iteratively seek the maximum axial force that can be applied such that the σ_{max} from Eq. (4) is the same as the product of yield strength and the maximum allowable HSR for the grade.
    - The axial force that satisfies the above criterion divided by the cross sectional area is the maximum allowable thermal stress.
    - This is then expressed as a *reduced* maximum allowable HSR, or a reduced allowable temperature.

The stress at which inelastic buckling occurs is usually close to the yield strength of the material. Thus, if the temperature change is such that yielding does not occur, inelastic buckling is unlikely[1]. If the temperature is higher than this limit (as it usually is), the unsupported section buckles and plastically deforms immediately thereafter. Eventually, as temperature continues to increase, the laterally deformed pipe makes contact with the outer constraint (in the case of a bulge), or pinches out when it contacts an inner constraint (in the case of an inward deformation). At the moment of contact, the shape of the deformed unsupported section may be approximated as a sinusoidal or polynomial curve, and can be calculated using five boundary conditions (zero lateral displacement and zero rotation at the fixed ends, and zero derivative at the point of contact). Although this allows for the calculation of strains for the application of a Low Cycle Fatigue design approach, damage grows very quickly with temperature after inelastic buckling. The further concern with excessive post-buckling plasticization with inelastic buckling is that the casing may tear at the crest of a kink due to excessive bending stress, or upon cool down, the combination of tensile stress and the moment caused by the tension in "opening" the bent shape can lead to tensile parting failure. For this reason, the limit in design is the onset of inelastic buckling.

3.4 Example

The effect of an un-cemented section on the maximum allowable temperature is illustrated in Figure 7 for a 9 5/8 in., 47 lb/ft (0.471 in. wall) L80 tubular in a 13 3/8 in. casing (radial clearance of 1.313 in.). This illustration uses the approach described above for the inelastic portion of the buckling, with helical buckling treated as described by Lubinski, et. al. (1962). As the figure shows, when the string is fully cemented, the allowable temperature change (ΔT_{max} = 244°C), according to the modified Holliday approach (maximum allowable stress ratio = 1.4) is at its highest, as expected. However, as the length of unsupported section is increased from zero, the maximum allowable temperature falls rapidly, reaching a low of 0.55 ΔT_{max}. This point represents the point at which the inelastic buckling load is at its lowest. As the unsupported length increases, and the buckling regime becomes elastic, the allowable temperature increases (since post-buckling bending stress increases linearly with axial force). This illustrates the danger of having short unsupported sections, and the less severe effect of long unsupported sections.

[1] This strategy of limiting the maximum temperature such that the material does not yield is one way to design for short (non-slender) unsupported sections. The reader will note that this is essentially the same as using Working Stress Design for thermal service.

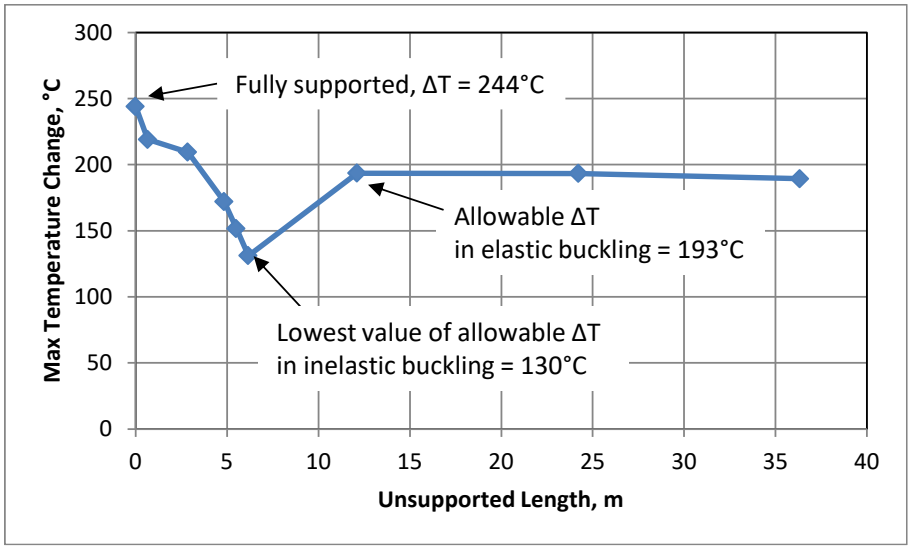

Figure 7. Effect of unsupported section on maximum allowable temperature, 9 5/8 in., 47 lb/ft, L80

3.5 Discussion

Inelastic buckling can occur in short, non-slender unsupported sections. These are usually a consequence of poor displacement and inadequate centralization during the primary cement job, or the use of top jobs to complete the cementing operation. It is also possible in acid zones where acid-resistant cement is not used, and the acid consumes a section of the cement, creating an unsupported section. This type of failure can occur in the tieback or liner.

Increase in yield strength[2] or wall thickness, or application of pre-tension during installation are two options for mitigation if the cement job is expected to be poor. Pre-tension may be difficult to implement, and even if it is feasible, it should be used with caution as it encroaches on the available tensile stress window for other drilling and production loads that increase pipe tension.

It is noted that most commercial programs do not consider inelastic buckling, and calculate the bending stress as if elastic buckling occurs, regardless of the length of unsupported section defined. The user must exercise care when interpreting such results. If an inelastic buckling model is not included, when short unsupported sections are expected, it is best to limit the temperature increase to just allow yielding (that is, disallow post-yield loading).

Trapped unsupported sections may also contain fluid which can respond to an increase in temperature by developing an increase in pressure. This pressure can also cause collapse of the inner casing, often much before inelastic buckling ensues. This is the subject of the next section. For now, it is relevant to observe that inelastic buckling usually occurs when trapped fluid pressure does not develop or is relieved. When trapped fluid pressure develops, the failure usually presents as a combination of collapse from the trapped pressure and inelastic buckling. Inelastic buckling failure almost always occurs in the very first heat half cycle. In all cases, the deformation is highly localized, with a kink or dent like presentation that looks much different from trapped pressure collapse. Parting failure localized at the site of inelastic buckling, if it happens, occurs at the first cool down, immediately after the kink appears in the pipe body.

3. ANNULAR PRESSURE BUILDUP INDUCED COLLAPSE

3.1 Description

Annular pressure buildup (APB) in trapped annuli is a common design consideration for subsea wells. The trapped annuli are created when a casing is not fully cemented, and the top of cement is shallower than the shoe of the outer casing forming the annulus. When the annulus is heated due to radial heat loss during production, the trapped fluid temperature increases, and the fluid expands in response. If some or all of this volumetric expansion is not permissible, pressure develops. The magnitude of APB depends upon the increase in temperature, fluid PVT properties, and the elastic response of the containing media, but it is quite large for typical fluids in annuli. While there are well documented methods to calculate the annular fluid expansion and the resultant APB, as a rule of thumb, the predicted APB pressures for typically used fluids is in the range of 1.0 to 1.8 MPa per °C temperature increase. This is clearly a substantial pressure increase, and quickly approaches the burst capacity of the outer casing or collapse capacity of the inner casing, threatening well integrity. As a result, APB in subsea wells, where the annuli cannot be relieved, often required the use of different mitigation techniques. Sathuvalli et al (2016) provide a comprehensive treatment of the selection, design and reliability of different APB mitigation methods. In land wells, APB is usually easily managed by relieving the pressure at the wellhead.

In geothermal and thermal service wells, the most common source of APB is trapped fluid pockets in the cement behind a tieback string (this is because APB in trapped pockets with access to formation often relieves itself by leaking off into the adjacent formation). Fluid pockets and mud channeling are a consequence of poor displacement of the drilling fluid by cement. If these pockets occur behind the tieback string, they become trapped with no path for relief, and quickly develop pressure when heated during production. For typically used production casings in geothermal wells, only 20°C to 30°C increase in temperature is

[2] Unlike elastic buckling, inelastic buckling is affected by yield strength

sufficient for the APB to exceed the collapse resistance of the casing. APB is relieved somewhat by cracking of cement and the (inward) deformation of the casing in response to the increase in pressure. Eventually, the deformation ceases when there is equilibrium between the pressure in the trapped pocket and the disallowed annular fluid expansion. For this reason, APB induced collapse does not always cause rupture or failure of the casing, especially when the trapped pockets are small in volume. Instead, it appears like a localized "protrusion" or inward bulge, compromising drift. An illustration of such a collapse is shown in Figure 8.

Figure 8. Illustration of APB induced collapse. Note the inward protrusion at the location of the collapse. There is no failure, but the protrusion compromises drift.

The volumetric relief required to relieve APB is usually very small, and can be calculated using the PVT behavior of the fluids, elastic properties of the surrounding solid media, and the initial and final average temperatures of the trapped pocket. For a 3 m (~10 ft) gap in a 9 5/8 in. by 13 3/8 in. annulus, the annular fluid expansion is only 3-4 liters.

Southon (2015) discusses APB induced collapse (or "casing implosion"), and his review of failure causes indicates that this is the most prevalent failure mode. Casings with local protrusions indicative of APB induced collapse are often clearly revealed by downhole videos. The authors have reviewed several such downhole video images. In these images, the bulge or protrusion is visible on one side of the casing circumference, over a 20° to 30° arc, and sometimes has an overhanging lip like appearance, probably due to the combined effect of inelastic buckling (compressive failure). Southon (2015) also discusses downhole video images, including one in which the casing was torn at the location of the failure, which is likely indicative of a combination of APB induced collapse and inelastic buckling over a relatively short unsupported length.

In most cases, APB induced collapse occurs in the very first heat half cycle (first production). Lentsch, et al (2015) present several examples of APB collapse, all of which occur during the first production. Lentsch et al (2015) also discuss APB induced collapse in some detail, and present several mitigation measures to combat this failure mechanism.

3.2 Mitigation of APB Induced Collapse

Unfortunately, the common APB mitigation approaches used in deepwater wells, such as vacuum insulated tubing, rupture disks and syntactic foams are not feasible options for mitigating the type of APB common in geothermal wells. The most obvious mitigation is to design and perform cement jobs such that no trapped fluid pockets are present. Southon (2005) suggests that using a tieback with a swellable packer to ensure good cement can avoid creation of trapped pockets. Lentsch, et al (2015) also discuss best practices in cementing to avoid creation of trapped pockets. However, APB induced collapse continues to occur in tieback casings. Cement formulations and slurry design are already well developed, so the main issues that remain are with cement placement. In general, the following steps may be considered in achieving a good cement job for tiebacks:

- Proper centralizer selection and placement. Centralizer standoff simulation models are commercially available, and should be used in designing centralizer placement.
- Proper cement displacement. Commercially available models can be used to simulate displacement efficiency. At a minimum, 100% excess should be used ensure complete displacement of the fluids. This is now a widely practiced measure in most geothermal fields.
- Proper slurry management. Minimize large variations in slurry density, or between between injected slurry density and return density, which are indicative of insufficient displacement. Care should be taken to ensure that the return density is within 0.024 SG (0.2 ppg) of the pumped slurry density.
- Use Acid Resistant Cement in acid-prone zones.
- Consider reciprocation and rotation of pipe during cementing to improve displacement efficiency.

Other cementing solutions have been described to combat APB induced collapse in the literature. Kruszewski and Witting (2018) mention reverse circulation of cement to improve placement efficiency and avoid top jobs. Brown et. al. (2016) discuss the use of engineered microspheres in cement to allow trapped annular fluid expansion and therefore relief of APB, thus protecting well

integrity. The method was developed for steam injection and cyclic steam stimulation wells, which also have the problem of APB induced collapse.

One architectural alternative to maintain well integrity (especially with regard to collapse of production tieback), is to design the well tubulars such that the outer string bursts (or connections in the outer string leak) before the inner string collapses, As the fluid expands in a trapped pocket, the cement cracks due to the resulting tensile hoop stress, and the trapped fluid may access the outer string, which, if designed to do so, can leak or rupture. The Code of Practice for Deep Geothermal Wells NZS 2403:2015 suggests that the collapse strength of the inner string should be at least 1.2 times the burst strength of the outer string (the quantitative basis of this recommendation is not clear). Southon (2005) argues that this may not always be practical, and may not even be enough to protect the inner string. This may be because as per the NZS procedure, the API burst of the outer pipe is compared to the API collapse of the inner pipe. However, the API Burst strength (or minimum internal yield pressure, as it is commonly known) is a thin wall, open ended yield equation, and is not a limit state equation. It therefore does not predict rupture. Thus, even if a ratio of 1.2 is maintained based on API performance properties, the inner casing is likely to still collapse before the outer casing ruptures.

In a recent paper, Suryanarayana, et al, (2020) present a quantitative design approach to allow outer casing rupture before inner casing collapse, thus maintaining well integrity. They show that a deterministic comparison of the API performance properties of the inner and outer casings, and maintaining a margin between the two, is not adequate to assure outer casing rupture before inner casing collapse. A more appropriate comparison would be between the limit state burst (Klever-Stewart Ductile Rupture) of the outer casing to the limit state collapse (Klever Generalized Tamano Collapse) of the inner casing. Both these limit states are discussed in detail in API TR 5C3 (ISO TR 10400). Further, as discussed in API TR 5C3, the material properties and geometric parameters used in calculating the limit states are all uncertain. Therefore, a probabilistic comparison between the inner casing collapse limit state and outer casing burst limit state is more appropriate.

For the trapped pocket to access the outer boundary, it must first fracture the cement. Suryanarayana, et al (2015) use a fracture mechanics approach and fracture toughness of typical geothermal cements to calculate a “critical APB”, that is, the APB at which the cement fractures. A second limit is the “Failure APB”, the APB at which the differential pressure across the outer casing is adequate to cause its rupture. The design criterion is then to ensure that the outer casing ruptures at the higher of the above two limits, before the inner casing collapses. Using limit states and probabilistic considerations, Suryanarayana, et al (2015) show how the inner and outer casing strings can be selected such that the probability of outer casing burst is much higher than the probability of inner casing collapse, thus assuring well integrity against APB induced collapse.

Both Southon (2005) and Kruszewski and Wittig (2018), as well as other workers (Lentsch, et al., 2015) implicate rapid heat up during production in the creation of conditions favorable for APB induced collapse. They propose instead a more gradual heat up in the first production, so that the tensile stress in the cement can cause cracks and micro annuli, and the resulting void volume created can help relieve APB when it occurs. This suggestion is yet to be quantitatively verified.

In summary, through cementing practices, appropriate tubular selection, and possibly operational constraints on the rate of first heat up, it is possible to mitigate APB collapse.

4. CORROSION AND ITS IMPACT ON COLLAPSE-LIKE FAILURES

Geothermal fluid chemistry is often corrosive. Materials selection usually takes this into account, and in some cases, non-ferrous alloys are indicated and used. Corrosion in geothermal wells is well recognized and always considered in design. A discussion of corrosion and corrosion modeling is presented in Suryanarayana and Krishnamurthy (2018). They recommend the use of commercial corrosion analysis programs like OLI (https://www.olisystems.com/), that model corrosion in aqueous solutions within a thermodynamic framework, and predict the rate of corrosion for a given material and fluid composition and chemistry. First, however, a rigorous analysis is required to ensure characterization of the water chemistry and the concentration of the dissolved gases. Hausler and Krishnamurthy (2017), discuss the need for full consideration of the solubility of acid gases as a function of temperature, pressure and chloride content. Sophisticated thermodynamic and process chemistry tools such as OLI make this possible. Inputs to this analysis include the fluid pressure, temperature, and phase behavior as a function of depth for different producing conditions. The main output of the analysis is a rate of corrosion in mm per year, or milli-inches per year (mpy).

4.1 Example

The procedure for corrosion analysis and wall loss estimation is illustrated for an example well. The basic well input data are shown in Table 3. The temperature and pressure are at the reservoir. Key chemistry details are shown in the table. As can be seen, in this case, the calculated pH (using OLI) is 4.04, while the field measured pH is 4.18.

Table 3. Basic Well Data for Corrosion Example

Input Data		
Reservoir Conditions		
Temperature	335	°C
Pressure	1750	psi
Chemistry		
CO_2	0.5	mole %
H_2S	0.05	mole %
Na	5900	mg/L
Cl^-	10800	mg/L
Boric Acid	2500	mg/L
$SO4^{2-}$	12	mg/L
HCO_3^-	25	mg/L
Calculated pH	4.04	
Field pH	4.18	

A thermo-hydraulic analysis is first performed using the expected flow conditions to determine the fluid behavior in the wellbore. The results are depicted in Figure 9. The left panel shows the temperature as function of pressure along the well, over the depth of interest. Both flowing and geothermal temperatures are shown. The flowing temperature varies between 335°C at the perforations, to about 310°C at the surface. Also shown is the phase of the fluid (marked using rectangular frames). In this well, steam breaks out at around 1,650 m, and the flow is two phase at shallower depths. The second panel shows the gaseous and aqueous volume as a function of depth at two temperatures, 310°C and 320°C. As can be seen, at depths shallower than 1100 m, the fluid is essentially gaseous in phase. These volumes are important in the analysis of dissolution in the liquid phase, and hence the corrosion wall loss. From these results, the chloride concentration can be calculated as a function of depth. The variation of chloride concentration in the liquid phase as a function of depth is shown in Figure 10. As the figure shows, chloride concentration increases rapidly in the two phase region, at low pressures and high temperatures.

These results are then used in OLI to calculate the expected rate of corrosion for a low-carbon steel (< 0.5% carbon). The rates of corrosion are shown in Table 4. These results show the minimum and maximum calculated corrosion rates over the range of temperature, pressure, phase and concentration conditions in the well over the region of interest. The maximum rate of corrosion is 40 mpy, and the minimum is 20 mpy. These rates are quite high (2-5 mpy is considered an acceptable rate of corrosion). With these rates of corrosion, the entire wall thickness (0.480 in.) is consumed in 19.2 years on average, and as quickly as in twelve years. Similar analysis can be performed with other alloys to aid materials selection if the available life is not adequate.

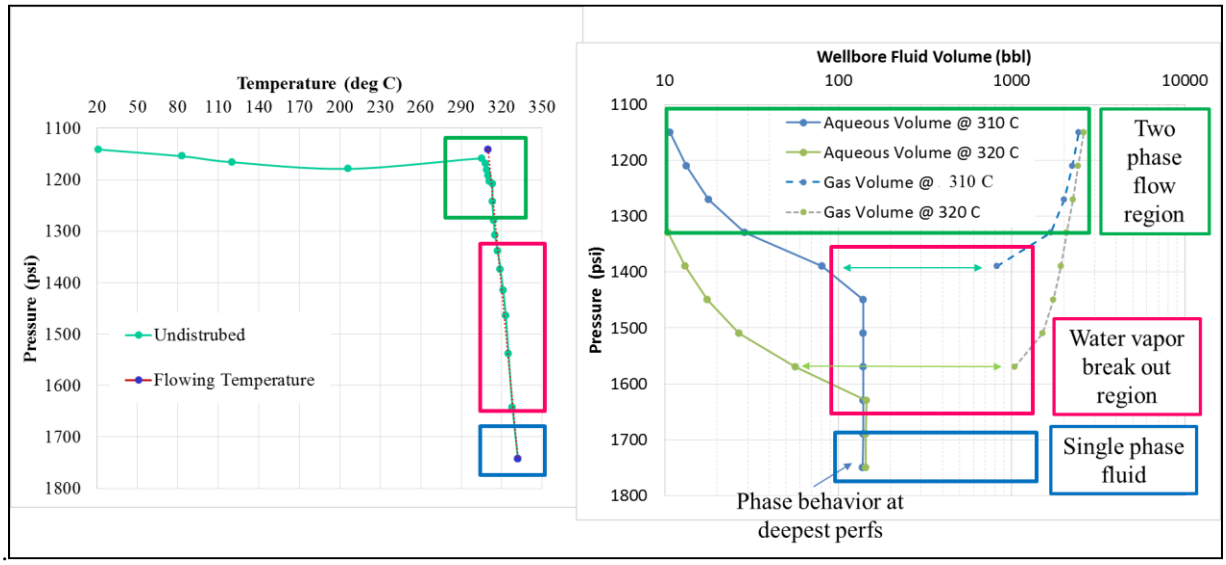

Figure 9. Thermo-Hydraulic analysis results for corrosion example- Temperature, pressure and gas/liquid volumes

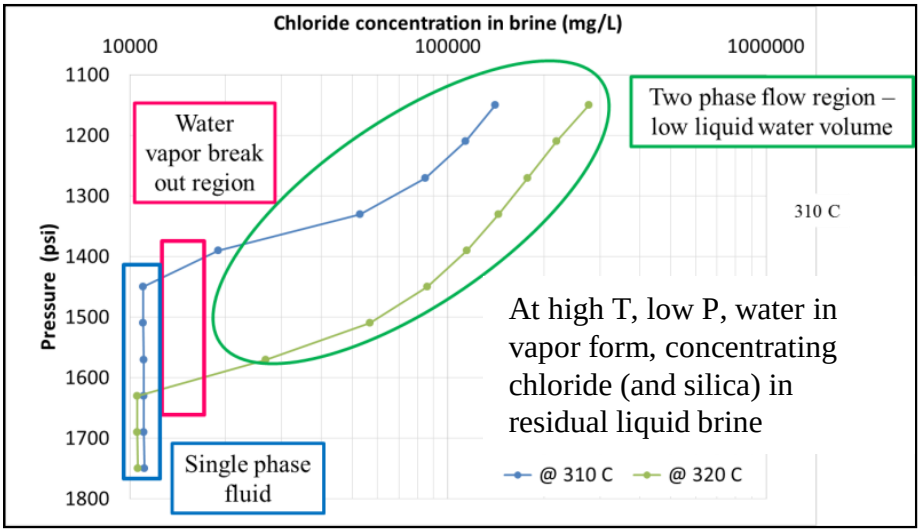

Figure 10. Chloride concentration variation as a function of depth

Table 4. Corrosion rate estimates

Results	
Max Corrosion Rate	40 mpy
Min Corrosion Rate	20 mpy
Average Rate	25 mpy
Wall thickness	0.480 in
Average Life	19.2 years
Min Life	12 years

4.2 Impact on Collapse Failure

In the preceding discussion, the life of the well is calculated as the time it takes for corrosion to consume all of the wall thickness. But much before this happens, corrosion wall loss affects the mechanisms of collapse failure discussed in this paper. In cold collapse, reduction in wall reduces the collapse resistance, and hence the resistance to cold collapse. If corrosion wall loss is expected, the remaining life in the context of cold collapse is the time it takes for the cold collapse safety factor (calculated as discussed in Sections 2.5 and 2.6) to fall below 5. In the case of inelastic buckling, wall thickness enters the calculation through Eq. (3). The onset of inelastic buckling is hastened by the reduced wall thickness. Finally, if a trapped pocket exists adjacent to a corroded section of the pipe, APB induced collapse is more likely. Therefore, it is important to use a corrosion analysis as a complement to the consideration of the collapse-like failure mechanisms discussed in this work.

5. CONCLUSIONS

In this work, after a brief overview of post-yield design approaches for thermal service tubulars, three mechanisms of collapse-like failure of geothermal well tubulars are discussed: cold collapse, inelastic buckling, and APB induced collapse. These failure mechanisms merit separate treatment because they are not covered by the post-yield design approaches.

Cold collapse, which is a combination of high tension and a collapse load, occurs in the cold half cycle, and can dictate tubular design. The problem is exacerbated in geothermal wells due to the deep water level upon cool down. The physical characteristics of cold collapse are discussed to aid recognition of this failure mode in failure investigations. A cold collapse design check is important for production casings and tiebacks in geothermal wells. A design criterion is presented and justified in the context of experimental and numerical analysis results. The method is simple to implement, and is illustrated through an example. An increase in the wall thickness (weight) of the tubular is the most effective way to satisfy cold collapse design requirements.

Inelastic buckling is a compressive failure mechanism that presents with collapse-like physical characteristics. It occurs in short unsupported sections, in response to thermally-induced compression. Short unsupported sections are usually a consequence of poor cementing. A method to calculate the inelastic buckling limit of short unsupported sections, based on the secant formula, is presented and illustrated via an example. It is shown that the impact of short unsupported sections is to significantly reduce the maximum allowable production temperature. Severe inelastic buckling (due to a combination of very short unsupported sections and high temperature) can cause tearing failure at the crest of the kink-like deformation caused by buckling, or tensile failure upon cool down. Improved cementing practices and increase in yield strength (or wall) are two ways inelastic buckling can be mitigated to allow higher temperature application. Pre-tension can also be considered.

Annular pressure buildup (APB) in trapped annuli is a familiar problem in subsea oil wells, and several mitigation methods have been developed. In geothermal wells, APB in trapped fluid pockets in the cement in tieback-casing (or casing casing) annuli is a common cause of collapse failures. Unfortunately, the mitigation measures developed for subsea wells are not feasible or applicable in geothermal wells. APB induced collapse usually occurs in the first heat half cycle, and depending upon the size of the pocket,

and available pressure relief from cracks and micro-annuli in the cement, causes inward deformation and failure of the casing. It sometimes occurs in combination with inelastic buckling. As in the case of inelastic buckling, a good cement job is the best mitigation approach. Elements of proper cementing, and the use of simulation tools to aid design of cementing operations, are discussed in the context of avoiding creation of trapped fluid pockets. Other mitigation approaches, including designing the annulus such that the inner casing collapse resistance is greater than the outer casing burst resistance, are discussed. It is argued that separation between inner casing collapse resistance and outer casing burst resistance should be based on the limit states, rather than API performance properties.

Corrosion wall loss affects all of the above failure mechanisms. The use of commercial software for corrosion analysis and prediction of expected wall loss are discussed, and an example of wall loss estimation is presented. The predicted wall loss can then be used in the design checks, and ensure that the well is designed to meet the production loads for the intended well life.

The failure modes and design checks discussed in this paper should be performed alongside post-yield design to ensure well integrity and obtain a robust well architecture. The authors hope that the paper provides an additional basis for the design of geothermal well tubulars that extends post-yield design approaches to improve lifetime integrity of geothermal wells.

6. ACKNOWLEDGEMENTS

The authors thank the management of Blade Energy Partners for supporting this work. The authors also thank Mr Rohit Swaminathan for his painstaking literature survey, and Mr Uday Arumugam for performing the finite element analysis in support of this work. Finally, the authors thank Ms Diya Yadav for creating the illustrations in this paper.

7. REFERENCES

API TR 5C3, “Technical Report on Equations and Calculations for Casing, Tubing and Line Pipe Used as Casing or Tubing; and Performance Properties for Casing and Tubing”, American Petroleum Institute, 2008 (Also see ISO TR 10400).

Brown, J., Kenny, N., and Slagmulder, Y., “Unique Cement Design to Mitigate Trapped Annular Pressure TAP Between Two Casing Strings in Steam Injection Wells”, *Society of Petroleum Engineers, SPE 184102*, Presented at the SPE Heavy Oil Conference and Exhibition, Kuwait City, Kuwait, December 2016.

Drilling and Completions Committee, “Heavy Oil and Oil Sands Operations, Industry Recommended Practice”, IRP Volume 3, 2002.

Fischer, F. D., Kolednik, O., Shan, G.X., and Rammerstorfer, F. G. , “A note on calibration of ductile failure damage indicators”, *International J. of Fracture,* 73, pp 345-357, 1995.

Gao, M., and Krishnamurthy, R. M., "Mechanical Damage in Pipelines: A Review of the Methods and Improvements in Characterization, Evaluation, and Mitigation", Chapter 22, in Oil and Gas Pipelines: Integrity and Safety Handbook, R. Winston Revie Ed., Wiley, April 2015.

Han, L., Wang, H., Wang, J., Xie, B., Tian, Z., and Wu, X., “Strain-Based Casing Design for Cyclic-Steam-Stimulation Wells”, *SPE Production and Operations Journal*, May 2018.

Hancock, J. W. and McKenzie, A. C. , “On the mechanisms of ductile failure in high-strength steels subjected to multi-axial stress-states”. *Journal of Mech. Phys. Solids*, Vol. 24, pp 147 to 169, 1976.

Holliday, G. H., “Calculation of Allowable Maximum Casing Temperature to Prevent Tension Failures in Thermal Wells”, *ASME Publications*, 69-Pet-10, 1969.

ISO/PAS 12835:2013 (TWCCEP), “Qualification of Casing Connections for Thermal Wells”. International Standards Organization, 2013.

Krishna, S., Milligan, R., George, K., Krishnamurthy, R. M., Powers, J., and Krener III, J., “Post Yield Strain Fatigue Experiments to Validate Low Cycle Methodology for Tubular and Connections”, *Society of Petroleum Engineers, SPE 193361*, 2018.

Kruszewski, M., & Wittig, V., “Review of failure modes in supercritical geothermal drilling projects”, *Geothermal Energy*, 6(1). doi:10.1186/s40517-018-0113-4, 2018.

Lentsch, D., Dorsch, K., Sonnleitner, N., and Schubert, A., “Prevention of Casing Failures in Ultra-Deep Geothermal Wells (Germany)”, Proceedings, World Geothermal Congress, Melbourne, Australia, 19-25 April 2015.

Lepper, G. B., “Production Casing Performance in a Thermal Field”, *Journal of Canadian Petroleum Technology*, Vol. 37, No. 1, September 1998.

Lubinski, W. S. Althouse, and J. L. Logan, “Helical Buckling of Tubing Sealed in Packers”, *Journal of Petroleum Technology*, June 1962, 655; Trans AIME, 225.

Maruyama, K., Tsuru, E., Ogasawara, M., Inoue, Y., and Peters, E. J., “An Experimental Study of Casing Performance Under Thermal Cycling Conditions”, *SPE Drilling Engineering*, June 1990. Also SPE 18776.

Mitchell, R. F., “New Concepts for Helical Buckling”, *SPE Drilling Engineering*, 303; Trans AIME 285, 1988.

Powers, J., Buell, S., Suryanarayana, P. V., and Sachdeva, P. , “Post-Yield Design of Thermal Service Tubulars and Connections - Case Studies”, *Society of Petroleum Engineers, SPE 182504*, 2016.

Rice, J. R., and Tracey, D. M., “On the ductile enlargement of voids in traxial stress fields”, *Journal of Mech. Phys. Solids*, Vol. 17, pp 201 to 217, 1969.

Sathuvalli, U. B., Pilko, R. M., Gonzalez, R. A., Pai, R. M., Sachdeva, P., and Suryanarayana, P. V., "Design and Performance of Annular Pressure Build-up Mitigation Techniques", *SPE 178886-PA, SPE Drilling and Completions*, September 2017.

Sathuvalli, Udaya B., Krishna, S., and Suryanarayana, P. V., "The Mechanical Response of Concentric Cemented Casings Exposed to Arbitrary Transverse External Geomechanical and Salt Loads", Society of Petroleum Engineers, *SPE 194121*, Presented at the SPE/IADC Annual Drilling Conference, Amsterdam, The Netherlands, March 2019.

Southon, J. N. A., "Geothermal Well Design, Construction and Failures", *Proceedings*, World Geothermal Congress, Antalya, Turkey, 24-29 April 2005

Sinclair Knight Merz, Box 9806, Auckland, New ZealandStandards New Zealand, "Code of Practice for Deep Geothermal Wells", New Zealand Standard NZS 2403:2015.

Suryanarayana, P. V. and Krishnamurthy, R. M.,"Strain-based and Low Cycle Fatigue Design Approaches for Thermal Service Tubulars", *SPE-178473*, presented at the SPE Thermal Well Integrity and Design Symposium, Banff, Alberta, Canada, 23–25 November 2015.

Suryanarayana, P. V., and Krishnamurthy, R. M., "Post-Yield Tubular Design and Material Selection Considerations for Improved Geothermal Well Integrity", *Proceedings*, 43rd Workshop on Geothermal Reservoir Engineering, Stanford University, Stanford, California, February 12-14, 2018, SGP-TR-213.

Suryanarayana, P. V., Bowling, J., Sathuvalli, U. B., and Krishnamurthy, R. M., "A Design Basis for Geothermal Well Tubulars Subjected to Annular Pressure Buildup from Fluids Trapped in Cement", Proceedings, 45th Workshop on Geothermal Reservoir Engineering, Stanford University, Stanford, California, February 10-12, 2020, SGP-TR-216

Teodoriu, C., " Why and When Does Casing Fail in Geothermal Wells: A Surprising Question?", *Proceedings*, World Geothermal Congress, Melbourne, Australia, 2015.

Teodoriu and G. Falcone, 2008, "Fatigue life predictions of a buttress casing connection exposed to large temperature variations". Proceedings of Thirty-Third Workshop on Geothermal Reservoir Engineering, SPG-TR-85.

Thorbjornsson, I., Kaldal, G., Gunnarsson, B., & Ragnarsson, À., "A New Approach to Mitigate Casing failures in High-Temperature Geothermal Wells", *GRC Transactions*,41, 2017.

Toscano, R. G., and Dvorkin, E. N., "Collapse of Steel Pipes under External pressure and Axial Tension", *Journal of Pipeline Engineering*, 4th Quarter, 2011.